SECURITY CLASSIFICATION OF THIS PAGE (When Data Entered)

REPORT DOCUMENTATION PAGE		READ INSTRUCTIONS BEFORE COMPLETING FORM
1. REPORT NUMBER JPL D-186	2. GOVT ACCESSION NO.	3. RECIPIENT'S CATALOG NUMBER
4. TITLE (and Subtitle) A NON-STANDARD PROBABILISTIC POSITION-FIXING MODEL		5. TYPE OF REPORT & PERIOD COVERED FINAL 6. PERFORMING ORG. REPORT NUMBER
7. AUTHOR(s) Prof. J. Ferling, Prof. L Knop, Prof. J. Denton, W. Duquette, L. Harris, Y. Lohse, S. Turicchi, D. Vela		8. CONTRACT OR GRANT NUMBER(s) NAS7-918
9. PERFORMING ORGANIZATION NAME AND ADDRESS Math Clinic, Claremont Graduate School Claremont McKenna College Claremont, CA 91711		10. PROGRAM ELEMENT, PROJECT, TASK AREA & WORK UNIT NUMBERS RE T&E AMEND # 187
11. CONTROLLING OFFICE NAME AND ADDRESS Commander, USAICS ATTN: ATSI-CD-SF Ft. Huachuca, AZ 85613-7000		12. REPORT DATE 30 June, 1985 13. NUMBER OF PAGES 38
14. MONITORING AGENCY NAME & ADDRESS (if different from Controlling Office) Jet Propulsion Laboratory ATTN: 126-200 California Institute of Technology 4800 Oak Grove Drive Pasadena, CA 91109		15. SECURITY CLASS. (of this report) UNCLASSIFIED 15a. DECLASSIFICATION/DOWNGRADING SCHEDULE
16. DISTRIBUTION STATEMENT (of this Report) Approved for Public Dissemination		
17. DISTRIBUTION STATEMENT (of the abstract entered in Block 20, if different from Report)		
18. SUPPLEMENTARY NOTES Prepared under contract to Jet Propulsion Laboratory for the US Army Intelligence Center and School's Combat Developer's Support Facility		
19. KEY WORDS (Continue on reverse side if necessary and identify by block number) DIRECTION FINDING,STANSFIELD'S MODEL,LINE OF BEARING,NORMAL DISTRIBUTION,ERROR DISTRIBUTION,BIVARIATE NORMAL DISTRIBUTION,CONFIDENCE REGIONS,CONFIDENCE ELLIPSES,PROBABILITY DENSITY,DENSITY FUNCTION,PROBABILITY REGIONS,TOLERANCE REGIONS		
20. ABSTRACT (Continue on reverse side if necessary and identify by block number) This is one of a series of algorithm analysis reports performed for the US Army Intelligence Center and School covering selected algorithms in existing or planned Intelligence and Electronic Warfare (IEW) systems. This report constructs a mathematical model of position fixing using one or two sensors for comparison with previously employed models. The impact of relaxation of certain assumptions in older models upon the derived confidence		

DD FORM 1 JAN 73 1473 EDITION OF 1 NOV 65 IS OBSOLETE

SECURITY CLASSIFICATION OF THIS PAGE (When Data Entered)

ellipses is examined, particularly with respect to the actual contained probability within the ellipses.

Keywords: radio direction finding; normal error distribution

JPL D-186

INSTITUTE OF DECISION SCIENCE
FOR BUSINESS & PUBLIC POLICY

A NON-STANDARD PROBABILISTIC
POSITION-FIXING MODEL

Conducted at

Institute of Decision Science
Claremont McKenna College

for

Mathematics Clinic
Claremont Graduate School

FINAL REPORT

Jet Propulsion Laboratory

June 1985

Claremont McKenna College
Claremont, California 91711

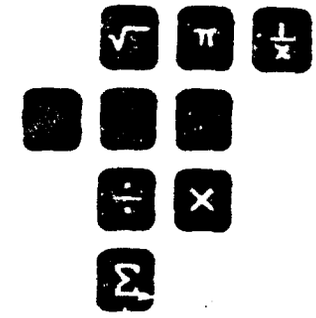

UAA 009

U.S. ARMY INTELLIGENCE CENTER AND SCHOOL
Software Analysis and Management System

A Non-Standard Probabilistic Position-Fixing Model

June 30, 1985

Concur:

James W. Gillis, Leader
Algorithm Methodology Subgroup

Edward J. Records, Manager
USAMS Task Team

J. P. McClure, Manager
Ground Data Systems Section

Yukio Nakamura, Manager
Defense Information Systems Program

JET PROPULSION LABORATORY
California Institute of Technology
Pasadena, California

PREFACE

The work described in this publication was performed at the Institute of Decision Science Claremont McKenna College, sponsored by the United States Army Intelligence Center and School. The writing and publication of this paper was supported by the Jet Propulsion Laboratory, California Institute of Technology, under a contract with the National Aeronautics and Space Administration.

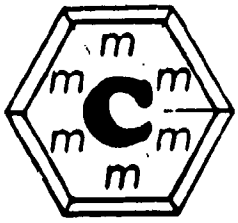

THE
MATHEMATICS CLINIC

CLINIC PARTICIPANTS

Will Duquette
Lisa Harris
Yvette Lohse
Scott Turicchi
Dan Vela

Professor James Denton : Faculty Consultant
Professor Larry Knop : Faculty Consultant
Professor John A. Ferling : Faculty Advisor

ACKNOWLEDGEMENTS

The Claremont Mathematics Clinic Team would like to express their appreciation to the Jet Propulsion Laboratory for the opportunity to be involved in this project. We would like to especially thank our JPL liaisons Martha Ann Griesel and James W. Gillis, as well as Sgt. Nick Sizemore. The Clinic has profited from their guidance, patience, and support.

The Clinic expresses a special thanks to Robert Walters, who enabled the Clinic members to produce plots of our work and allowed us to make use of the Rose Institute's digitizer.

TABLE OF CONTENTS

I. Introduction

This is the final report of the CGS/CMC Mathematics Clinic. Our project was for the Ground Data Systems section of the Intelligence Analysis Group at the Jet Propulsion Laboratory. Our project concerned the gathering of intelligence information through radio direction finding and fixing. We focused on the way radio sensors may be used to locate radio emitters such as radio transmitters or radar sets, and on errors in the readings returned by such sensors. The goal was to use this information, taking into account various errors, so that a region can be mapped around an estimate of the emitter location such that the true location of the emitter lies in this region with a specified probability.

We examined two models of a simple intelligence gathering scenario, both of which were restricted to the two-sensor case. The first was based on the classical assumptions of df fixing originally proposed by R.G. Stansfield. The second was a model constructed by the Clinic, which was created by relaxing one of Stansfield's simplifying assumptions. Our analysis of these models revealed that this particular assumption of Stansfield's introduces an additional error which is eliminated in the model constructed by the Clinic. The goal of this analysis was to critique the methods currently used to find confidence regions about location estimates.

In this report, we first discuss Stansfield's model as applied to the two-sensor case and its implications for the construction of confidence regions. Second, we describe our modification of the classical model, and certain subsequent analytical complexities. Third, we present the methods that we employed to mitigate the effects of these complexities. Fourth, we compare the results of our model with those of the Stansfield model. We then examine other types of errors originating from the radio sensors and their placement, and show in particular that a two-dimensional error in the location of a sensor is equivalent to a one-dimensional angular error -- a special case of our general model. In addition we will discuss several related topics, including a one-sensor model, systematic error, and the use of a digitizer or other computer analysis aids. Finally, we discuss areas for future research and state our final conclusions.

II. Stansfield's Model

The classical df fixing model was studied by R.G. Stansfield during World War II. Here we use a simple case of the general model with two radio sensors and a single emitter. In Figure 1 the sensors are denoted by S1 and S2, and the emitter is labeled E. Each sensor detects the radio signals broadcast by the emitter and returns an estimate of the line of bearing from the sensor to the emitter. The angles the true lines of bearing make with the baseline are denoted by Mu(Alpha) and Mu(Beta) respectively. However, it is improbable that the sensors would ever return exactly these lines of bearing, due to a variety of factors such as operator error, equipment error, terrain effects and atmospheric conditions. We will group these effects under the heading "measurement error."

The question arises as to how this measurement error is quantified. Clearly, these errors will be in degrees since the readings returned by the sensors are themselves in degrees. However, in order to simplify the analysis, Stansfield made a number of important assumptions, which are enumerated below. Assumption (3) is particularly relevant at this point.

(1) The earth is flat near the true position of the transmitter.

(2) The bearing lines are straight.

(3) An error of observation displaces the bearing line parallel to itself.

(4) Errors in separate bearings contributing to a fix are independent.

(5) The errors are normally distributed about a mean of zero, and the variances are known.

The third assumption is significant, and is detailed in Figure 2. Suppose that sensor 2 has returned the true line of bearing from itself to the emitter, while sensor 1 is in error. That is, sensor 1 returns the angle Alpha, and thus the line of bearing in Figure 2 labeled L2. Examination of these readings would place the estimate of the emitter's location at E'. Now, this is where Assumption 3 makes itself felt. Rather than measuring the error in sensor 1's reading by the difference Mu(Alpha) - Alpha, Stansfield draws a new line through point E' parallel to the true line of bearing from sensor 1 to the emitter. He measures the error, D1, in terms of the distance

between the true line of bearing and its parallel displacement at E'. Put another way, the error D1 in sensor 1's reading is the perpendicular distance from E' to the true line of bearing. Errors in the reading from sensor 2 are dealt with similarly.

The essence of Stansfield's simplifying assumption is this -- the error in a sensor reading may be measured by this parallel displacement (or perpendicular distance) without regard for the corresponding angular error. Further, he makes the following assumption about the nature of the error: the distance between the true line of bearing and the parallel displaced line follows the normal probability law with a mean of zero and some known standard deviation. Since this assumption is assumed to hold for both sensors, the estimate of the location will follow the bivariate normal probability law. The density function for this distribution is shown in Equation 1.

$$(1) \qquad f_{\alpha,\beta}(\alpha,\beta) = \frac{1}{2\pi\sigma_\alpha\sigma_\beta} \exp\left[-\frac{1}{2}\left(\frac{\alpha-\mu_\alpha}{\sigma_\alpha}\right)^2 - \frac{1}{2}\left(\frac{\beta-\mu_\beta}{\sigma_\beta}\right)^2\right]$$

This is a desirable result as the bivariate normal is a well-understood probability law with many useful properties. Thus, the above simplifying assumption has ramifications for the estimate of the emitter location, which includes both the point estimate and the confidence region.

We must digress momentarily to define these terms. The point estimate is simply the most likely position of the emitter given the sensor readings. Due to the error in the sensor readings, it is unlikely that the point estimate will exactly equal the true location of the emitter. This is why confidence regions are constructed. The region estimate, or confidence region, measures how far the point estimate is likely to be from the true position of the emitter. In Figure 3 there is a 95% confidence ellipse of the type that one would calculate using the Stansfield model. As before, E represents the emitter, and E' the point estimate of the emitter's location. The meaning of this ellipse is that if one estimates the location of the emitter 100 times, and constructs a confidence ellipse each time, one would expect about 95 of the confidence ellipses constructed to contain point E.

While the confidence region in this example is an ellipse, confidence regions can take many different shapes. In Figure 3, both the ellipse and the square are 95% confidence regions. Since the ellipse captures the same probability in a smaller area, it is a better estimate of the error in our point estimate. In fact, this is the definition of an optimal confidence region: it is that region which captures the desired level of confidence in the smallest area.

Because of the assumption of parallel error displacement,

the optimal confidence region in Stansfield's model is an ellipse having the formula shown in Equation 2.

(2) $$n\left[\left(\frac{\alpha-\bar{\alpha}}{\sigma_\alpha}\right)^2 + \left(\frac{\beta-\bar{\beta}}{\sigma_\beta}\right)^2\right] \leq \chi^2_{2,a}$$

This is the ordinary confidence region associated with the bivariate normal distribution.

III. Modifications: The Clinic's Model

As is the case with any theoretical research, it is interesting to drop assumptions and determine whether the conclusions are significantly altered. In studying this location problem, the Clinic retained the assumptions enumerated above with the exception of Assumption (3) -- the parallel error displacement assumption. In its place we use the more natural assumption of angular error displacemnt. That is, we measure the error in a sensor reading by the number of degrees that it deviates from the true line of bearing -- the difference Mu(Alpha) - Alpha. Further, we assume that this error is normally distributed with a mean of zero and some known standard deviation. Figure 4 shows an example of this model. As in Figure 2, the true lines of bearing have angles Mu(Alpha) and Mu(Beta) with the baseline. Sensors 1 and 2 return the angles Alpha and Beta respectively, yielding the estimated emitter location E'. The measurement errors in these readings are Mu(Alpha) - Alpha and Mu(Beta) - Beta.

Because we have assumed that the error is angular and not a parallel displacement distance, it can easily be shown that the distribution of the emitter location estimate about the true location of the emitter is no longer the bivariate normal. The nature of the distribution is shown by the following analysis.

Since we have assumed that these errors are normally distributed about a mean of zero, we know that 95% of the readings will fall within $\pm$ 2 standard deviations of the true line of bearing. In all of our examples we have arbitrarily chosen a standard deviation of 1 degree. Thus, if Mu(Alpha) = 80 degrees and Mu(Beta) = 110 degrees, then we would expect 95% of the readings for sensors 1 and 2 to fall between 78 and 82 degrees, and 108 and 112 degrees respectively. Similarly, 99% of the readings should fall within 3 standard deviations -- between 77 and 83 for sensor 1, and 107 and 113 for sensor 2. The bearing lines associated with these extreme values give us the large quadrilateral in Figure 5. Further, we know that this quadrilateral contains about 98% (.99 x .99) of the emitter estimates. To obtain a rough estimate for the probability density we constructed lines of bearing corresponding to errors of $\pm$ 0.5, $\pm$ 1.0, $\pm$ 1.5, $\pm$ 2.0, $\pm$ 2.5, and $\pm$ 3.0. These rays divide the large quadrilateral into 25 small quadrilaterals, as shown in Figure 5.

As the next step, we found the probability of a location estimate falling into each of these small quadrilaterals. Because of symmetry in the angular error distribution (the

normal), corresponding quadrilaterals will have equal probabilities. For instance, the uppermost and bottommost quadrilaterals in Figure 5, both labeled Y, have the same probability. It is clear, however, that their areas are very different. We termed this array of quadrilaterals with assigned probabilities a probability grid.

These quadrilaterals marked Y have the same probability, 0.003672, but their areas are 3410.3 and 1587.7 respectively. Thus, the average probability density in these regions are 0.00000108 and 0.00000232 -- which differ by a factor of 2. Clearly the distribution of the location estimates about the true location is skewed.

This shows that even when the angular error for each line of bearing is normally distributed., the points of intersection of these lines of bearing do not have a bivariate normal distribution. Finer grids of more than 3600 small quadrilaterals were produced both graphically and analytically by computer. Both methods showed evidence that the points were not distributed according to the bivariate normal probability law. Because the density function is not the bivariate normal, there is no reason to believe that the best confidence regions are elliptically shaped.

IV. Methods to Determine Functional Form

The Clinic used the probability grid derived above to explore the shape of the density function in a number of ways, including strips of probability and bands of equi-density.

As was stated in the previous section, if the bivariate normal function were used, then the large quadrilateral would be symmetrically shaped and any two corresponding quadrilaterals, such as those in Figure 5, would have the same average probability density. If bands of equi-probability were graphed so that only those points satisfying a given inequality were plotted, one would expect to see the points evenly distributed above and below the true emitter location. When angular displacement is used, it is clear that the points are not equally distributed about the true emitter location. If fact, if regions of relatively high density are graphed, then the majority of the plotted points will lie below the intersection of the true lines of bearing. Conversely, if low density regions are graphed, then the majority of the points will lie above the intersection of the true lines of bearing. This tells us that regions above the true location have lower density than those below.

Examining the "strips" shown in Figure 6 yielded similar results. These strips were constructed so as to divide the distribution into a number of bands of equal width both above and below the true location of the emitter. The probability of any reading falling into each of these strips was calculated using a probability grid. If the distribution were the bivariate normal, we would expect corresponding strips above and below the true emitter location to have about the same probability. Table 1, however, shows a case in which the skewness of the distribution is quite clear.

Having tried other techniques to determine the shape of the probability function and its corresponding confidence regions without much success, the Clinic decided to investigate transforming the probability funtion from the angular to the rectangular coordinate system. This is equivalent to transforming the bivariate normal (Equation #1). The transformation for the X and Y coordinates are given below:

$$(3) \qquad X = \frac{D \tan \beta}{\tan \beta - \tan \alpha} \qquad Y = \frac{D \tan \alpha \tan \beta}{\tan \beta - \tan \alpha}$$

or inversely,

$$\alpha = \tan^{-1}\left(\frac{Y}{X}\right) \qquad \beta = \tan^{-1}\left(\frac{Y}{X-D}\right) \tag{4}$$

To obtain the joint density of X and Y we use the following transformation formula:

$$f_{X,Y}(X,Y) = f_{\alpha,\beta}\left(\tan\frac{-Y}{X},\ \tan\frac{-Y}{X-D}\right)|J| \tag{5}$$

where $|J|$ is the determinant of the following matrix:

$$\begin{bmatrix} \frac{\partial\alpha}{\partial X} & \frac{\partial\alpha}{\partial Y} \\ \frac{\partial\beta}{\partial X} & \frac{\partial\beta}{\partial Y} \end{bmatrix} = \begin{bmatrix} \frac{-Y}{X^2+Y^2} & \frac{X-D}{X^2+Y^2} \\ \frac{-Y}{(X-D)^2+Y^2} & \frac{X-D}{(X-D)^2+Y^2} \end{bmatrix} \tag{6}$$

Solving, this gives us

$$J = \frac{Y\ D}{(X^2+Y^2)\left[(X-D)^2+Y^2\right]} \tag{7}$$

Using these transformations and the bivariate normal it is possible to rewrite the equation in terms of X and Y. The result is presented below:

$$f_{X,Y}(X,Y) = \frac{1}{2\pi\sigma_\alpha\sigma_\beta}\left|\frac{Y\ D}{(X^2+Y^2)\left[(X-D)^2+Y^2\right]}\right| \cdot \exp\left\{-\frac{1}{2}\left[\left(\frac{\tan^{-1}\frac{Y}{X}-\tan^{-1}\frac{Y_0}{X_0}}{\sigma_\alpha}\right)^2+\left(\frac{\tan^{-1}\frac{Y}{X-D}-\tan^{-1}\frac{Y_0}{X_0-D}}{\sigma_\beta}\right)^2\right]\right\} \tag{8}$$

where (X_0, Y_0) corresponds to (μ_α, μ_β).

However, this density function is not easy to analyze either analytically or numerically. Therefore, the Clinic transformed the optimal confidence region from the angular coordinate system, using the same relationships for X and Y. This yielded the following inequality:

$$(9) \qquad n\left[\left(\frac{\tan^{-1}\frac{Y}{X} - \tan^{-1}\frac{Y_\emptyset}{X_\emptyset}}{\sigma_\alpha}\right)^2 + \left(\frac{\tan^{-1}\frac{Y}{X-D} - \tan^{-1}\frac{Y_\emptyset}{X_\emptyset - D}}{\sigma_\beta}\right)^2\right] \leq \chi^2_{2,\alpha}$$

When the boundary points of this inequality are graphed, the region is nearly, but not quite elliptical.

Since it was not possible to tell visually how significantly these regions differed from ellipses, the Clinic performed a least squares analysis on the regions. First, we generated 50 boundary points from the original angular confidence inequality. These points were then transformed into the XY coordinate system using the transformation formulas. These are the data that were used in the regression.

The general form of a quadratic equation in the XY system is given below:

$$(10) \qquad A'X^2 + B'XY + C'Y^2 + D'X + E'Y + F' = \emptyset$$

Manipulating this equation yields a form which can be estimated by the techniques of ordinary least squares.

$$(11) \qquad X^2 = -BXY - CY^2 - DX - EY - F$$

where $B = B'/A'$, $C = C'/A'$, $D = D'/A'$, $E = E'/A'$ and $F = F'/A'$.

While this estimated ellipse is only an approximation to the transformed region, it is quite close. For example, when we estimated a 95% confidence ellipse in the angular coordinate system for the Mu(Alpha)=80 degree / Mu(Beta)=110 degree case, the estimated ellipse using regression contained 95.011% of the probability. Such a small deviation from the desired 95% can be accounted for by numerical errors inherent in the method employed, as well as the grid size used. Due to the closeness of

the approximation, and the difficulties in analyzing the transformed regions, it is these ellipses, determined by linear regression which we will use to contrast with the Stansfield ellipses.

V. Comparison of the Confidence Region Methods

We have now examined two distinct methods of constructing confidence regions: Stansfield's and the Clinic's. In this section we shall compare the results obtained from both methods when they are applied to the Clinic's version of the two-sensor model. The results show that while the Clinic's method is not necessarily the optimal method of constructing confidence regions given our model, it is a better method than Stansfield's. That is, the Clinic's confidence regions capture a given amount of probability in a smaller area than do Stansfield's.

The first method is that formulated by Stansfield, based on his parallel displacement assumption. Since this assumption allows the bivariate normal distribution to be used, the optimal confidence region is the ordinary ellipse based on this distribution. However, if the parallel displacement assumption is dropped, and our model used in its place, the Stansfield confidence ellipse is no longer optimal. Instead, we propose the "transformed" region which was derived in the previous section by transforming the optimal ellipse in angular coordinates into a region in rectangular coordinates.

As we have discussed, this transformed region is almost, but not quite, elliptical. In the numerical examples presented here we have used our least-squares approximation to the transformed region.

At this point we must digress momentarily to consider the relationship between confidence regions and probability regions, which are sometimes known as tolerance regions. An example of a probability region is one of the quadrilaterals in our probability grid. Based on a certain probability distribution, it contains a certain amount of probability. A 95% probability region is simply a region which contains 95% of the distribution's probability. An optimal probability region we define as that region which contains the desired probability with the smallest area. By contrast, the optimal 95% confidence region is that region with the smallest area which will catch the true location of the emitter 95 times out of one hundred.

The relationship between these is that the optimal way of constructing a probability region about the true location of the emitter is also the optimal way of constructing a confidence region about an estimate of the emitter's location. This assumes that the probability region is based on the sampling distribution, but this is irrelevant since the sampling and the base distributions are the same when only one observation is

taken irrelevant. The result is that instead of constructing confidence regions we may construct probability regions using the same methods, and arrive at valid conclusions. All of the analysis in this section was done using probability regions.

In particular we shall focus on the case where the true lines of bearing from Sensors 1 and 2 are 80 degrees and 110 degrees respectively. Further, the sensors are 1000 meters apart, and the error for both sensors has a standard deviation of 1 degree.

Figure 7 contains a graph of the 50%, 75% and 95% probability ellipses calculated using the classical method, and Table 2 lists their area and the probability contained in them. Note that they are concentric and centered at the true emitter location. Notice further that they do not contain the correct amount of probability. In fact, they tend to contain about 25% less probability than they ought to. This is because Stansfield's ellipses are inappropriate when the angular error is normally distributed.

The graphs of the 50%, 75% and 95% regions calculated using the Clinic's method are shown in figure 8, and their areas and probabilities are listed in Table 3. Due to the skewness of the density function, these regions are not centered at the true emitter location. Rather, the higher the desired level of confidence the further the region is positioned from the baseline. These regions, which are only approximations, contain close to the correct probability. In fact, the differences are small enough to be indistinguishable from numerical errors inherent in our methods of analysis. The use of a probability grid, for example, guarantees that our program will return values good only to a few decimal places.

Also included in Tables 2 and 3 are figures for the 70 degree/170 degree and 45 degree/135 degree cases. The related ellipses are graphed in Figures 9, 10, 11, and 12. Please note that the scale of the drawing varies from figure to figure, so direct comparisons of size are difficult. The "area" values in Tables 2 and 3 should aid comparison. These results strongly indicate that using the Stansfield model brings unnecessary error into the process of construction confidence regions.

V. Sensor Location Error

Thus far, we have discussed the angular measurement error that can occur from a given sensor reading. However, other types of error are also encountered, such as sensor location error.

Sensor location error occurs when the actual location of the sensor differs from the reported location of the sensor. For example, suppose it is believed that the sensor is located at position S1 in Figure 13 when, in fact, it is at point A. The effect is that the reported angle, and consequently line of bearing, will be applied to the point S1 instead of A. The result is that the estimated location is E' instead of E. Thus, the estimate of the emitter location has shifted from E to E' because of the location error.

To analyze the effect of this error, the Clinic began by assuming that the distribution of the sensor location error follows the bivariate normal probability law. Then, we constructed a circle with a radius of 3.5 sigma about the sensor. Due to the characteristics of the normal probability distribution, we know that there is a 99% probability that the sensor lies within the circle. However, it is not necessary to use a two dimensional region such as a circle to have a 99% probability. Note that any point on or within the circle has a corresponding counterpart on the baseline. Hence, if the sensor is located anywhere on the leftmost dotted line, it will return the same reading for the line of bearing. Thus, we need to include only the point A' in the analysis. Similarily, this is true for any sensor position. As a result, we are able to restrict the analysis to the points that lie on the baseline.

For a given point on the baseline, a line can be drawn to the true emitter location. The angle that is formed with the baseline is the reported angle. It is this angle that is then applied to the point S1, which is where the sensor is believed to be. The resulting estimate of the emitter is E' (See Figure 14).

It becomes of interest to examine the distribution of these angles for a given sensor location. Thus, a portion of the baseline (at least three sigma) was subdivided into fifteen equally spaced intervals. A line segment was constructed from the midpoint of the interval to the true emitter location. From this, the angle that is formed by this line segment and the baseline can be calculated. Each of these intervals has a probability associated with it, and this probability corresponds to the angle as well. This distribution of angles is plotted in Figure 15 along with the normal distribution having the same mean

and sigma values. As this diagram shows, the distribution of the angles is very close to normal. Thus, we have demonstrated that the sensor location error problem is equivalent to the angular measurement error discussed earlier, and the distribution of the angles about the mean is approximately normal.

VI. Other Topics

During the course of the year the Clinic also examined a number of other topics, including a one-radar scenario, systematic error due to equipment bias, and the potential use of a digitizer or similar hardware by an intelligence analyst.

The one-radar scenario is based on the Clinic's two-sensor model, and follows all of the same assumptions. The only difference is the nature of the sensor. In the two-sensor case, each sensor returns a single line of bearing. Thus, two sensors are required to locate an emitter. In the one-radar scenario, shown in Figure 16, we use a full radar set in place of a sensor. Since the radar is not merely a passive receiver of radio signals, but also a transmitter, it is able to supplement the line of bearing with a distance reading along that line of bearing.

In Figure 16, the emitter is denoted by E (actually, it could be any object large enough to register on a radar), and the radar is denoted by S. The line SE is the true line of bearing from the radar to the emitter, and the length of line segment SE is the true distance, r. The angle the true line of bearing makes with the baseline is a. In this figure a reading has been taken, returning the values (r',a'), and the resulting estimate of the emitter's location is E'.

If Stansfield's assumptions are applied to this model, only one is modified -- that of parallel error displacement. Instead, error is measured in the natural units: degrees for the angle reading and meters for the distance reading. Further, we assume that the error in both of these readings is normally distributed around zero error with some known standard deviation.

The analysis done on this model was based on a probability grid completely analogous to that used in the two-sensor case. Such a grid is shown in Figure 17. As before we calculated the probability of a reading falling in each of the small regions, and used this to approximate the density function. While the grid shown has only 25 sub-regions, that actually used in the computer analysis had over 3600.

While this is less complex problem mathematically than the Clinic's two-sensor model, it is clear from the grid that many of the same comments apply. For example, the distribution of radar readings certainly does not follow the bivariate normal distribution; as in the two sensor case corresponding sub-regions have differing areas, and so the density function is

skewed. While we did no further analysis, we expect that the location of confidence regions constructed for this model would depend on the level of confidence, just as in the two-sensor case. However, if the distance r is large enough compared to the possible errors in the angle and distance readings, it is possible that the bivariate normal distribution may be a good approximation to the true density. More research would be required to determine exactly when this might be the case.

The other type of error that the Clinic began to investigate is systematic error. This error occurs when the readings from the two sensors are perfectly correlated. This situation happens when the same piece of equipment is used to take both readings, due to inherent equipment bias. It was not possible to treat this subject in the depth desired. This topic will be pursued further next year.

Lastly, the Clinic considered in limited detail a related problem: that of terrain features. The area contained by a confidence region may include a lake, gorge, or other natural area in which one would hardly expect to find an emitter. Yet the confidence region assumes that every point within it is a possible location. One would deal with the problem by using conditional probability techniques. That is, there are ways of calculating the confidence that the emitter is in the region, while taken into account that fact that it cannot be in the middle of a lake. The difficulty is that terrain features seldom have mathematically pleasing shapes, and are thus hard to work with. One solution to this problem involves the use of a computer input device called a digitizer.

While a lightpen could also be used, the Clinic had access to the digitizer at the Rose Institute, a research institute at Claremont McKenna College. With this device a map of the terrain could be placed on the digitizer table, and a "picture" of the probability distribution "overlayed" on it by the computer. An analyst would then be able to specify very irregular regions by drawing on the digitizer table with an electronic stylus. Lakes and other features could be easily blocked out.

The Clinic wrote a small amount of rather limited software for this purpose, drawing on a private software library produced by the Rose Institute. This software was sufficient for our research, but not for the task outlined above. We believe that this is an idea worth pursuing in the future.

VII. Conclusion

In its analysis, the Clinic has relied on extremely simple models, with no more than two sensors, to examine and critique the classical sensor/location problem first studied by R.G. Stansfield. Yet even with such models, the effect of modifying Stansfield's parallel error displacement assumption is striking. When the methods used by Stansfield for constructing confidence ellipses is used with the probability density derived by the Clinic, the results are decidedly far too optimistic. As we believe that our modification is the natural way to relax Stansfield's assumption, our results could conceivably be quite important for practical intelligence gathering systems.

It is difficult, if not impossible, to predict how our modification would effect situations with three or more sensors, especially since different intelligence systems deal with multiple sensors in different ways. However, it is clear that it would be dependent upon the configuration of the sensors; a triangle of sensors centered on the emitter might conceivably mitigate the error, whereas three sensors all arrange on one baseline might even worsen the error. Further, while the Clinic has studied several different sources of errors, little has been done to consider them together. It may be a decidedly ghastly brew.

Finally, the Clinic chose to take only one observation from the sensors in their analysis, as it was believed that individual readings would not likely be independent. It is possible that with more observations the differences between the two sorts of confidence regions would grow less; it is also possible that errors would multiply. At any rate, it is clear that a sizable amount of research remains.

TABLE 1:

Probability Strip Analysis

The following table contains the results of a probability strip analysis performed on the 80 degree / 110 degree case. The standard deviation of the errors was assumed to one degree for both sensors, and the width between the sensors was 1000 meters.

The left column shows the probability contained in the strips below the true location of the emitter; the right column shows the probability in the corresponding column above. As is easily seen, the strips just below the emitter contain more probability than those just above. Thus, the density is skewed.

Lower Strips	Upper Strips
0.2025	0.1976
0.1723	0.1609
0.0828	0.0768
0.0306	0.0435
0.0060	0.0160

Width of strips = 50 meters

TABLE 2:

Areas and Contained Probabilities for Stansfield Ellipses

	True Lines of Bearing (in degrees)		
	MA=80; MB=110;	MA=70; MB=170;	MA=45; MB=135;
95% Confidence			
Area:	20887	303	1433
Probability:	77.173%	58.264%	77.629%
Center: X Coord.	326.35	60.31	500.00
Center: Y Coord.	1850.83	165.69	500.00
75% Confidence			
Area:	9665	140	663
Probability:	49.618	34.142%	49.774%
Center: X Coord.	326.35	60.31	500.00
Center: Y Coord.	1850.83	165.69	500.00
50% Confidence			
Area:	303	70	331
Probability:	28.834	18.495%	29.635%
Center: X Coord.	326.35	60.31	500.00
Center: Y Coord.	1850.83	165.69	500.00

Note: All figures in this table were calculated under the assumption that the two sensors were located 1000 meters apart, and that the standard deviation of the error in the sensor readings was one degree. Distances are in meters and areas are in square meters.

TABLE 3:

Areas and Contained Probabilities for the Clinic's Ellipses

	True Lines of Bearing (in degrees)		
	MA=80; MB=110;	MA=70; MB=170;	MA=45; MB=135;
95% Confidence			
Area:	43257	989	2949
Probability:	95.002%	95.011%	95.379%
Center: X Coord.	324.36	60.90	499.88
Center: Y Coord.	1875.51	167.27	500.52
75% Confidence			
Area:	19800	455	1364
Probability:	75.015	75.027%	75.711%
Center: X Coord.	325.44	60.58	499.94
Center: Y Coord.	1862.16	166.42	500.25
50% Confidence			
Area:	9884	227	692
Probability:	50.096	50.230%	50.867%
Center: X Coord.	325.90	60.44	499.98
Center: Y Coord.	1856.50	166.06	500.13

Note: All figures in this table were calculated under the assumption that the two sensors were located 1000 meters apart, and that the standard deviation of the error in the sensor readings was one degree. Distances are in meters and areas are in square meters.

Figure 1

Stansfield's Two-Sensor Model

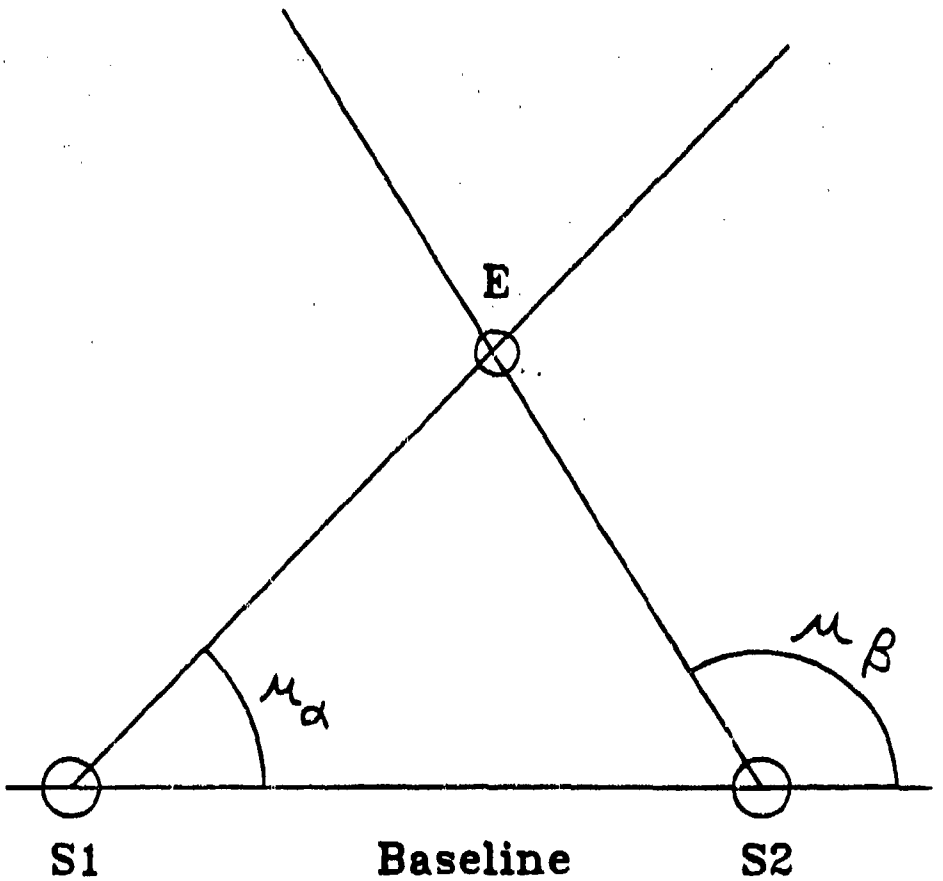

Figure 2

Stansfield's Two-Sensor Model

Error Displacement

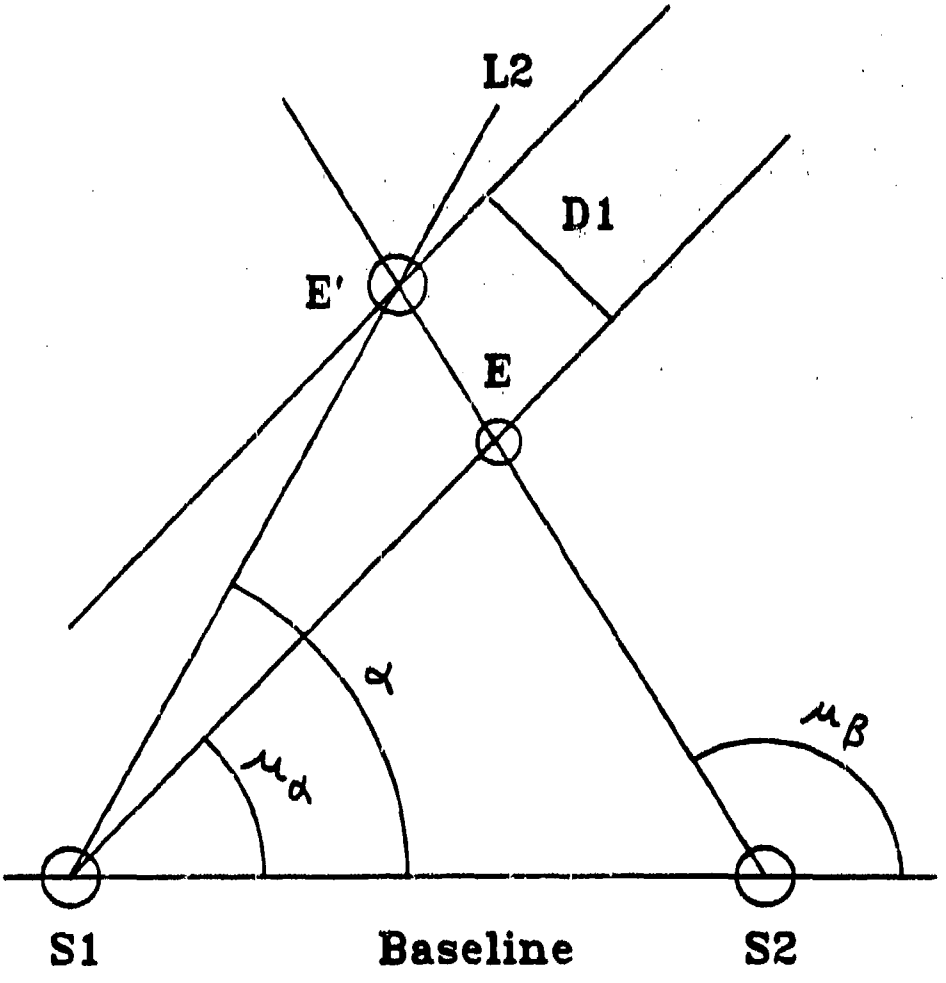

Figure 3

TWO 95% CONFIDENCE REGIONS

Figure 4

The Clinic's Two-Sensor Model

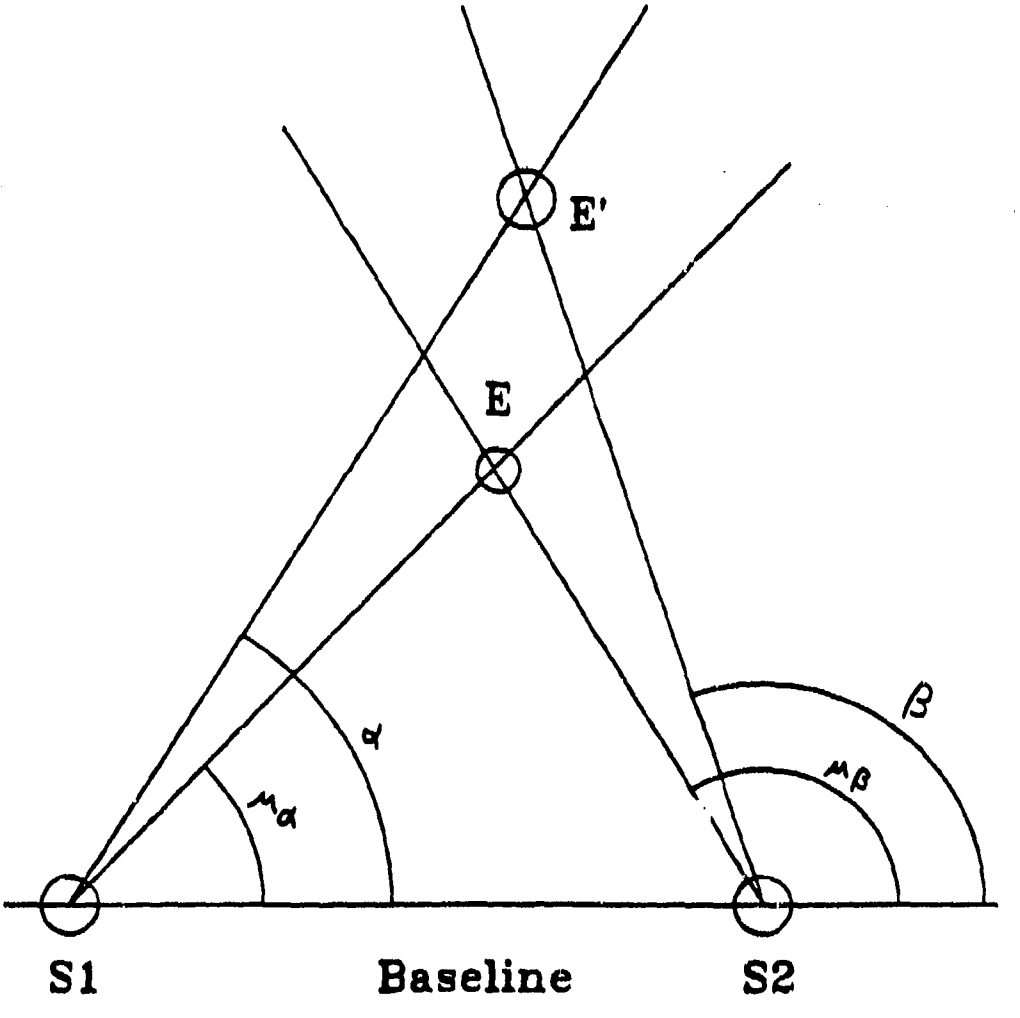

Figure 5

The Clinic's Probability Grid

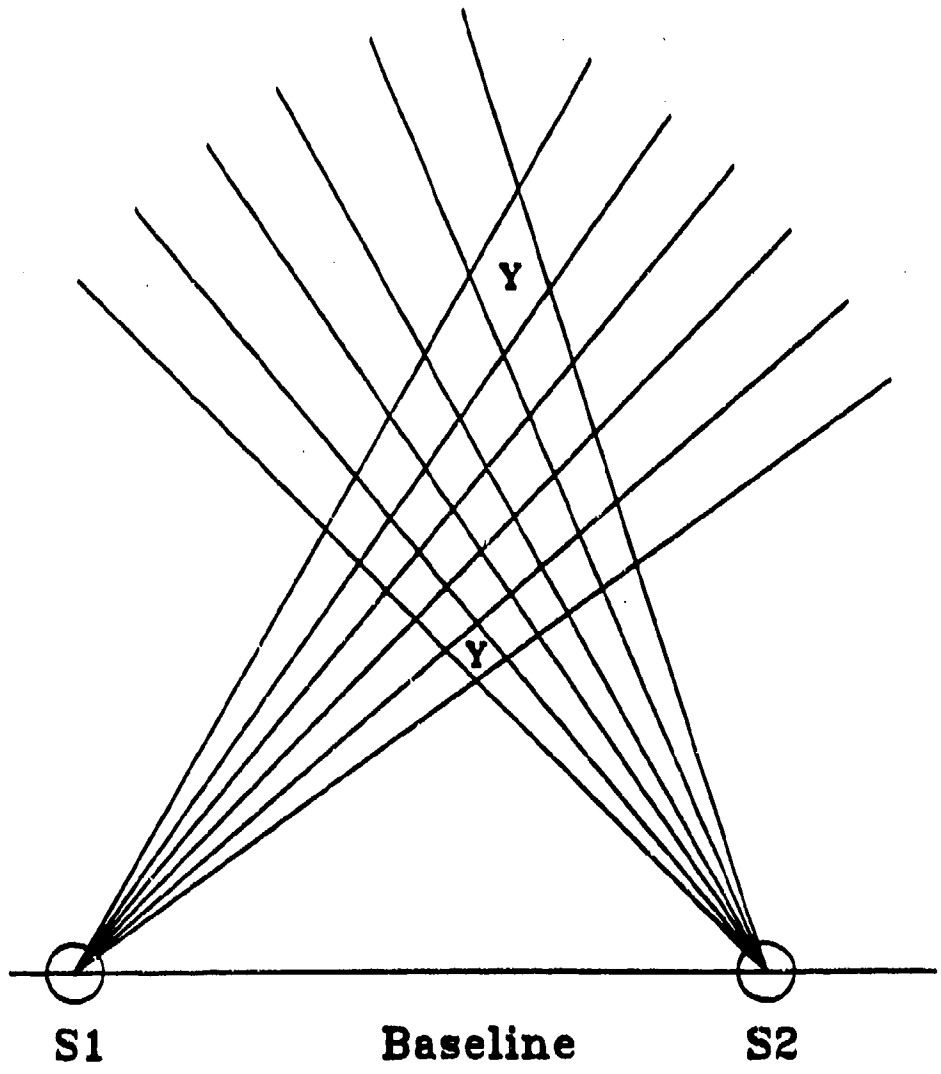

Figure 6

Probability Strip Analysis

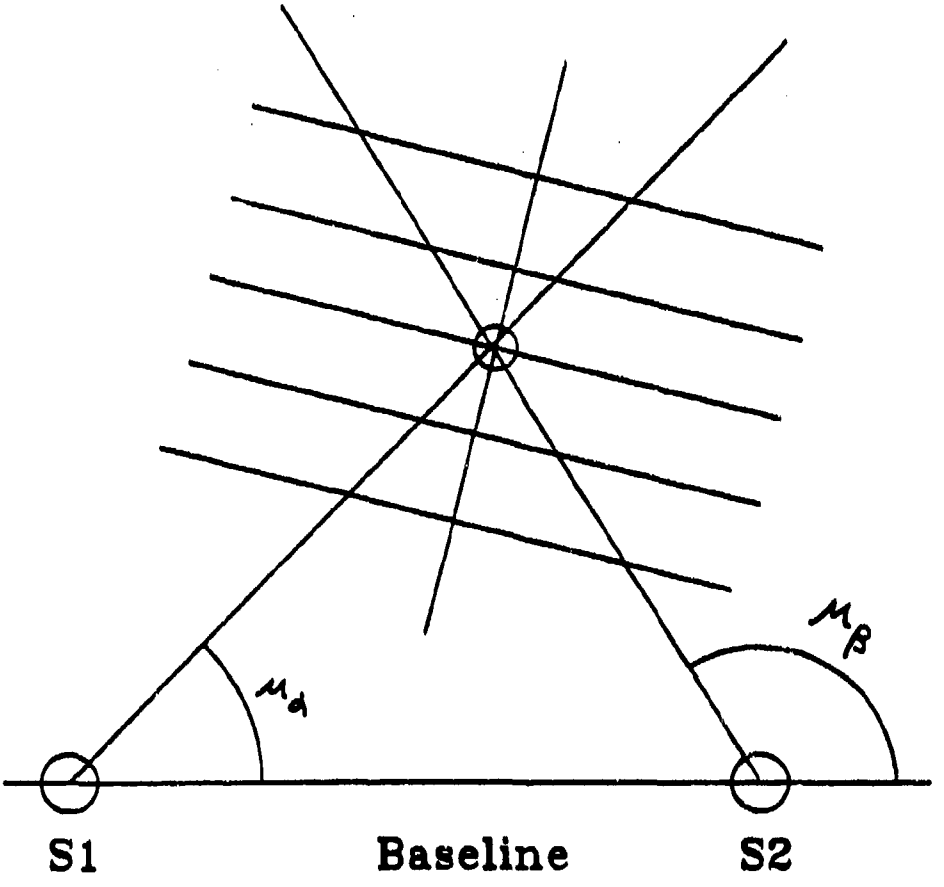

Figure 7

Stansfield's Confidence Ellipses for
the 80 degree / 110 degree case.

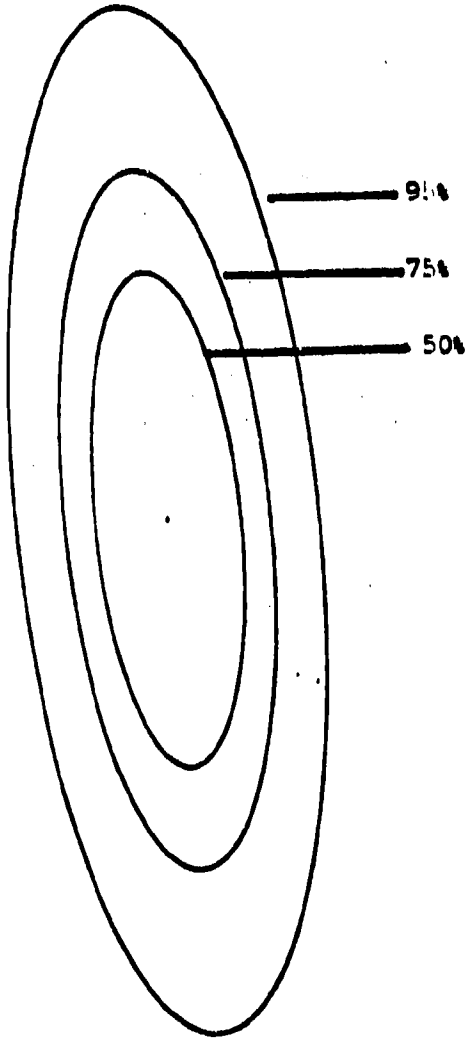

Figure 8

The Clinic's Confidence Region for the 80 degree / 110 degree case.

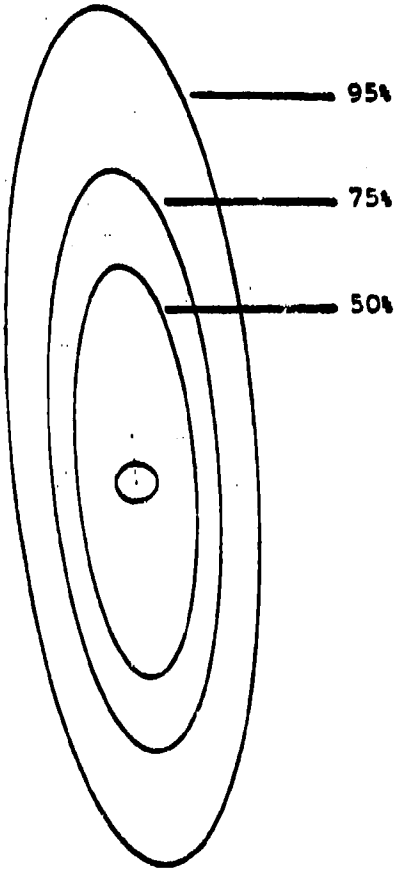

Figure 9

Stansfield's Confidence Ellipse for
the 70 degree / 170 degree case.

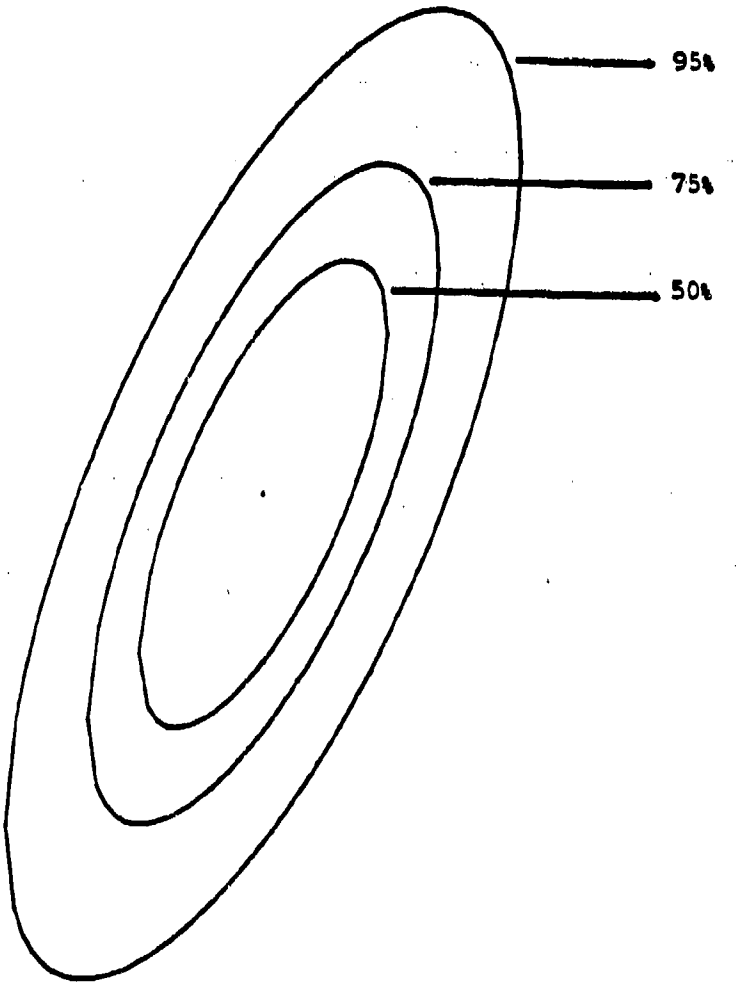

Figure 10

The Clinic's Confidence Region for the
70 degree / 170 degree case.

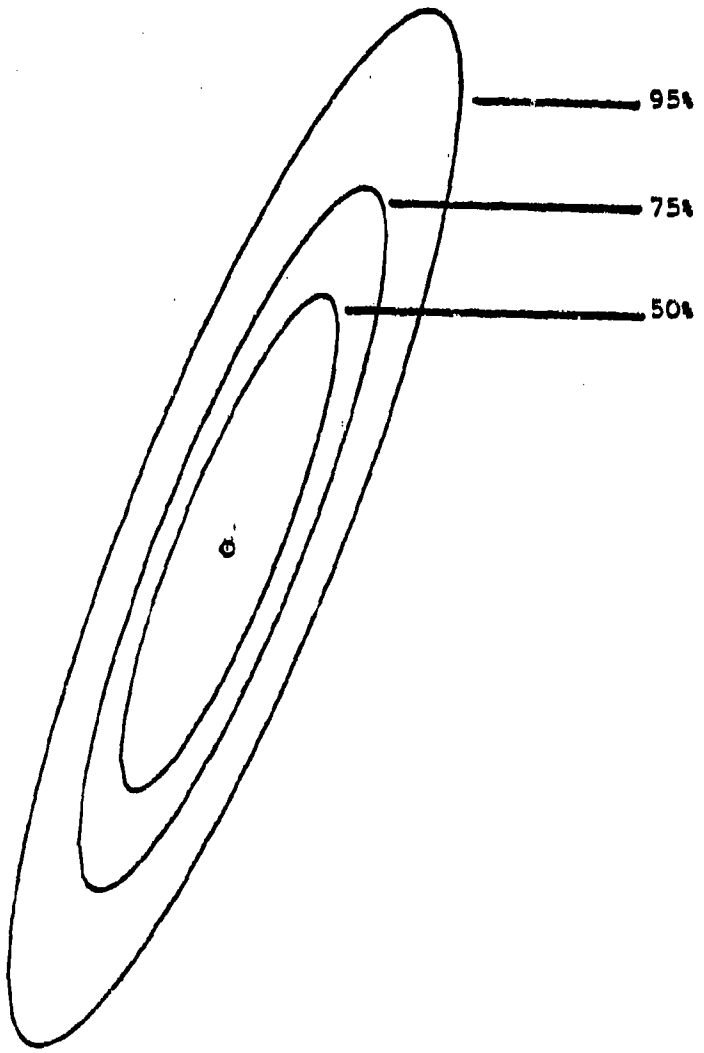

Figure 11

Stansfield's Confidence Ellipses for
the 45 degree / 135 degree case.

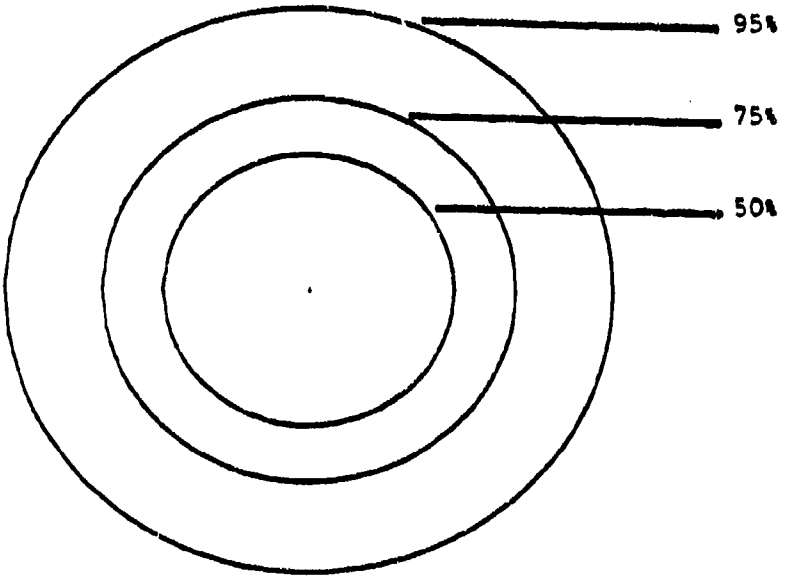

Figure 12

The Clinic's Confidence Regions for the
45 degree / 135 degree case.

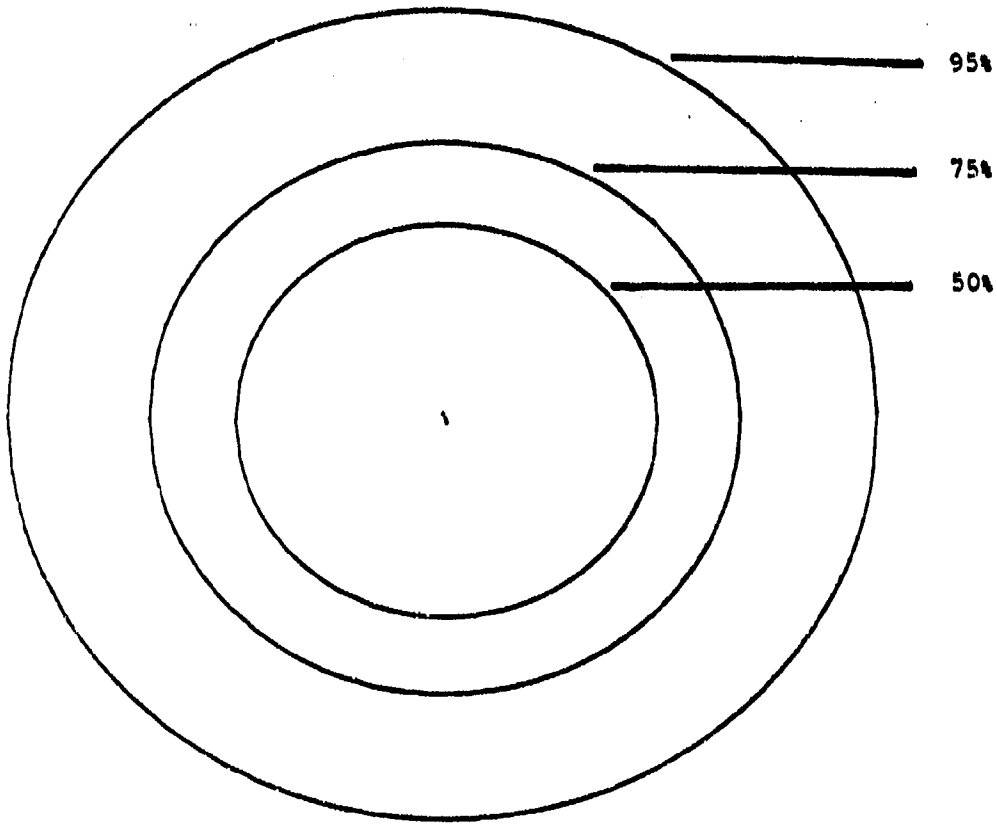

LOCATION ERROR MODEL

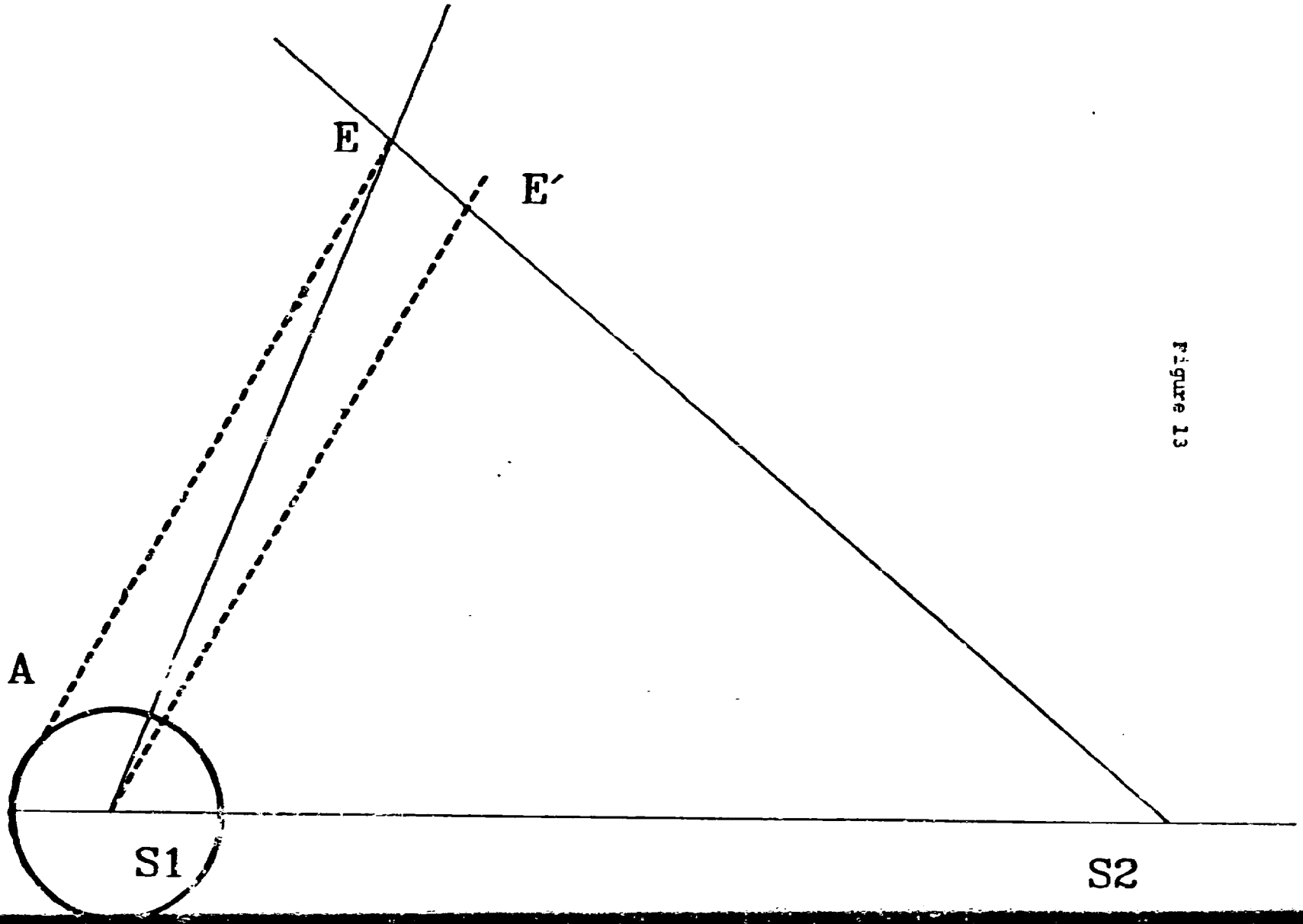

Figure 13

LOCATION ERROR MODEL

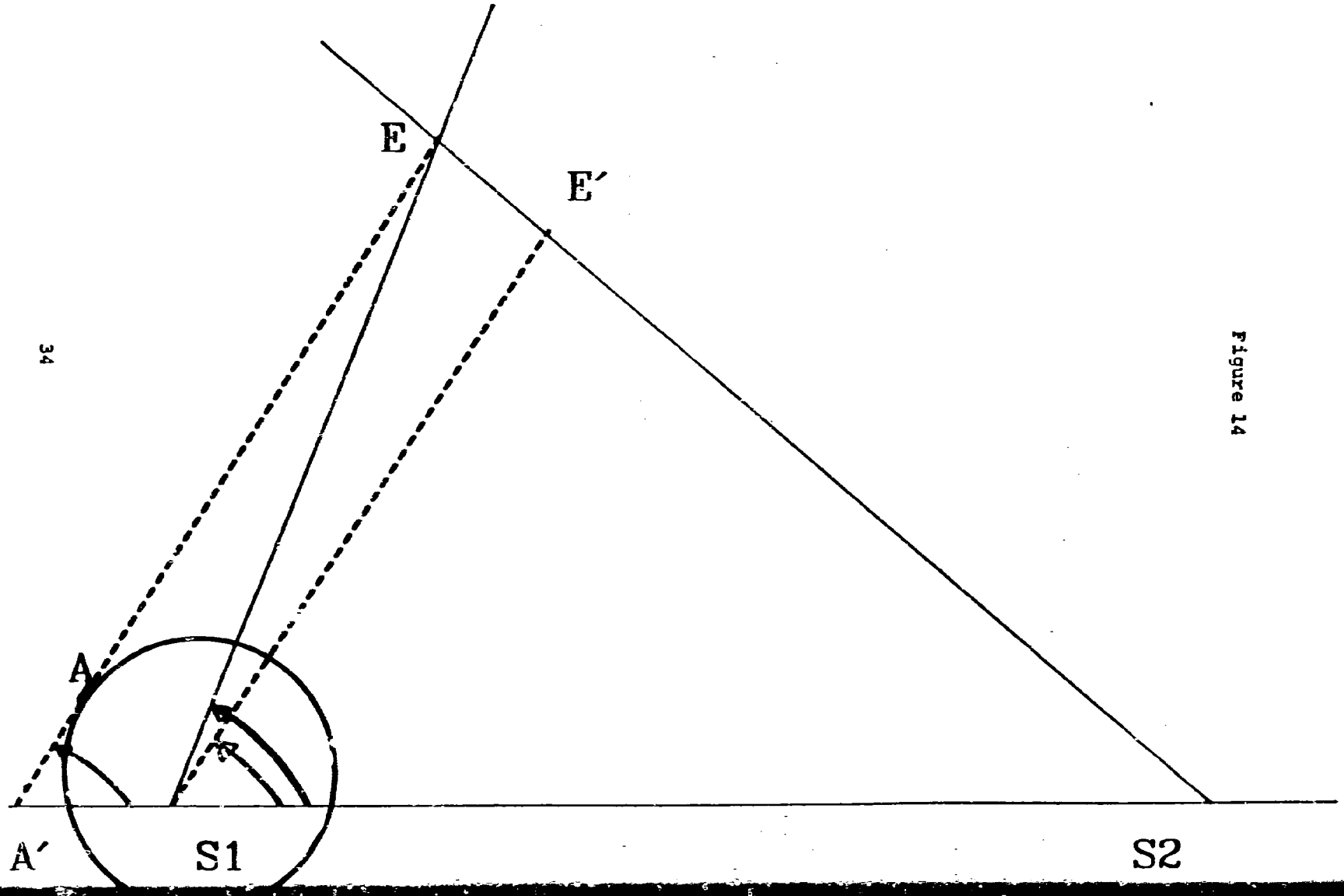

Figure 14

LOCATION ERROR ACTUAL DISTRIBUTION

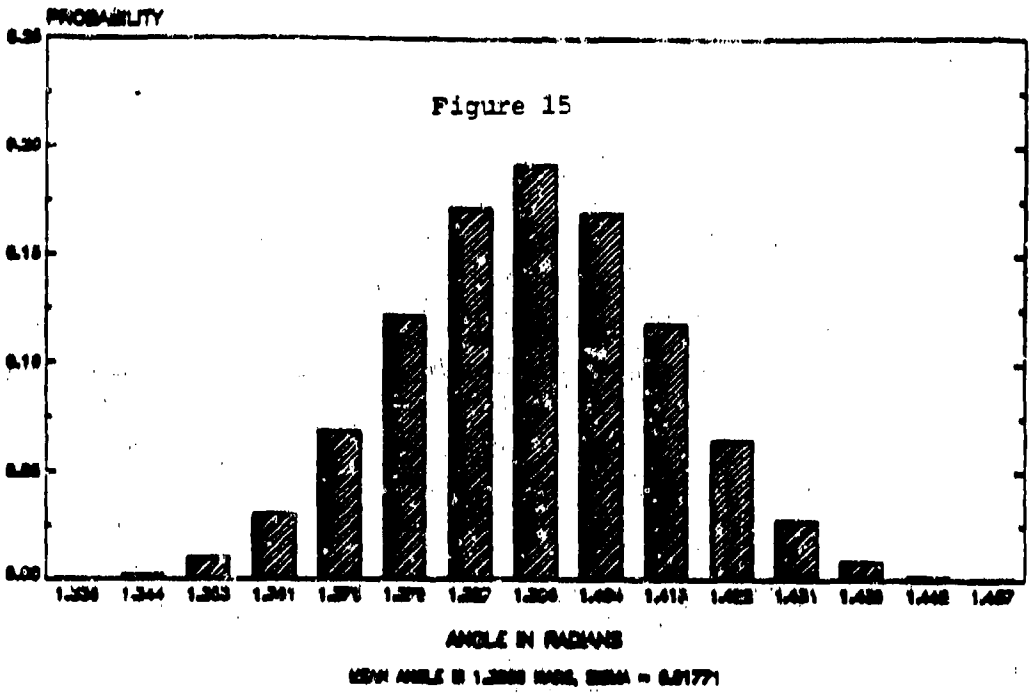

Figure 15

LOCATION ERROR NORMAL DISTRIBUTION

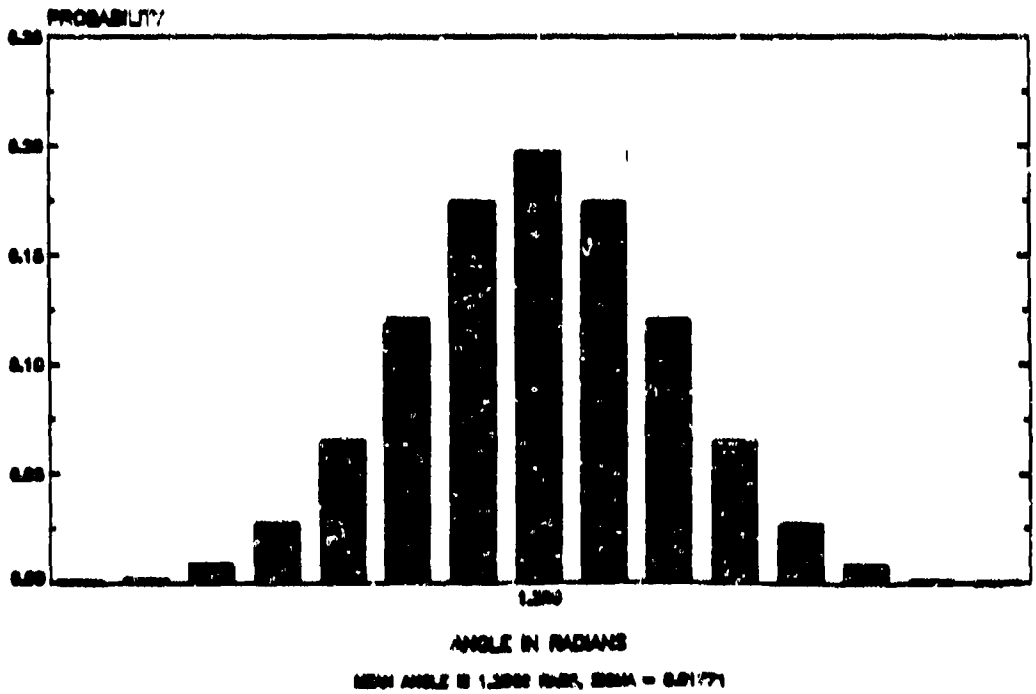

Figure 16

The Clinic's One-Sensor Model

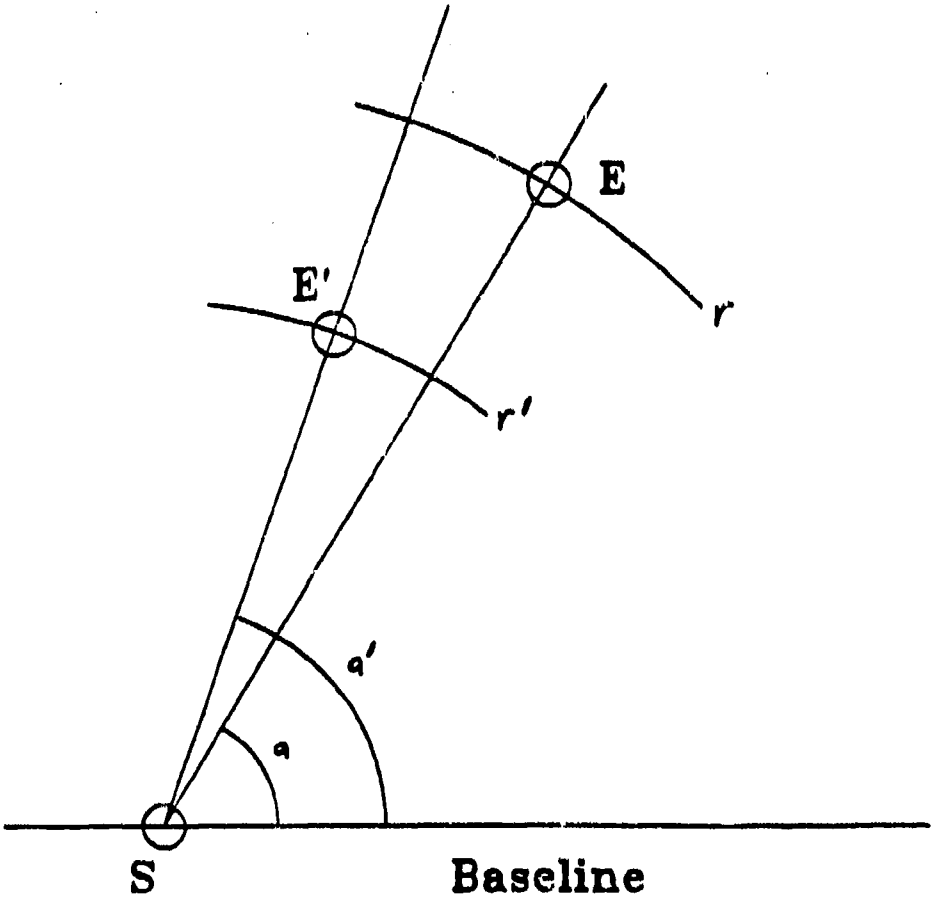

Figure 17

One-Sensor Probability Grid

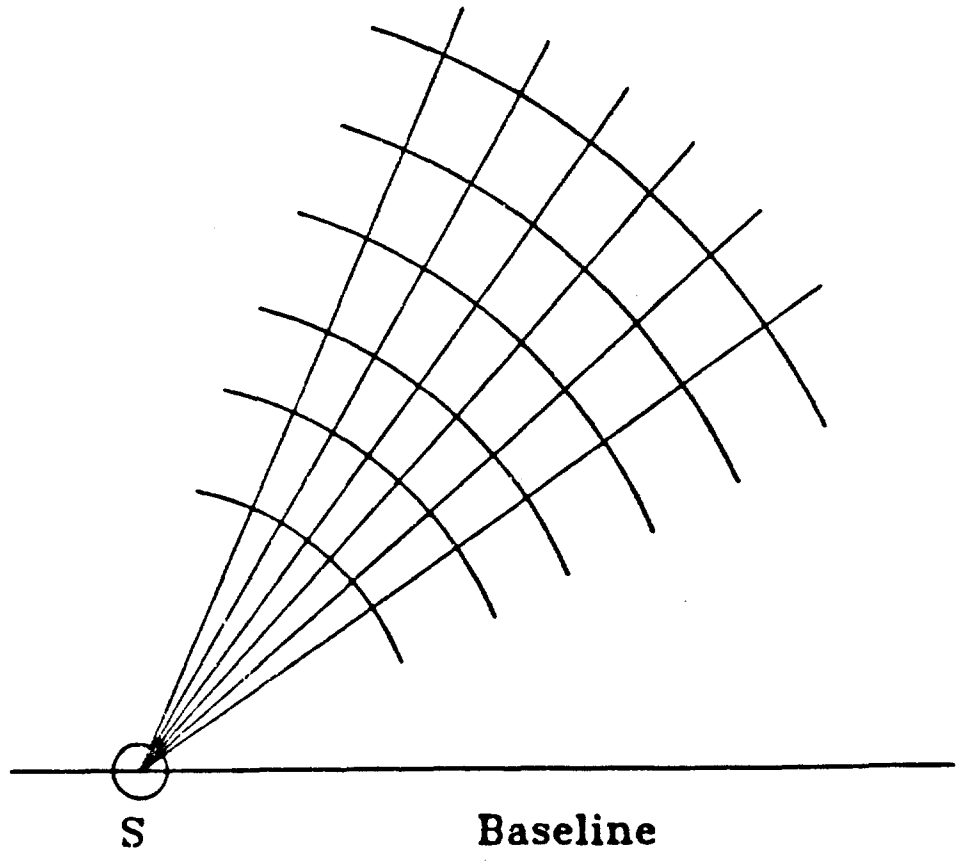

REFERENCES

1. Stansfield, R.G. "Statistical Theory of D.F. Fixing." (March 1947):762-770.

2. Daniells, H.E. "The Theory of Position Finding." The Journal of the Royal Stat. Soc. Series B, 13:2 (1951).

3. Gething, P.J.D. Radio Direction Finding. (London: Controller HMSO, 1978).